Research Article | Vol. 29, No. 7 / 29 March 2021 / Optics Express 9699
Optics EXPRESS

High-efficiency vertical fibre-to-polymer waveguide coupling scheme for scalable polymer photonic circuits

ABHAI KUMAR,[1,2,3] SIDDHARTH NAMBIAR,[1,3] RAKSHITHA KALLEGA,[1,3] PRAVEEN RANGANATH,[1] PRIYA EA,[1] AND SHANKAR KUMAR SELVARAJA[1,*]

[1]*Center for Nanoscience and Engineering, Indian Institute of Science, Bangalore 560012, India*
[2]*Now at Defence Materials Stores Research and Development Establishment-DRDO Labs, Kanpur, 208013, India*
[3]*Equal contribution*
[*]*shankarks@iisc.ac.in*

Abstract: Polymer photonic circuits offer a versatile platform for various applications, including communication, sensing and optical signal processing. Though polymers offer broadband, linear and nonlinear optical properties, the coupling between an optical fibre and a polymer waveguide has been a challenge. In this work, we propose and demonstrate a wafer-scale vertical coupling scheme for polymer waveguides. The scheme uses a silicon nitride grating coupler with an inverse taper to couple between an optical fibre and a *SU*8 polymer waveguide. We demonstrate a maximum coupling efficiency of -3.55 dB in the C-band and -2.92 dB in the L-band with a 3-dB bandwidth of 74 and 80 nm, respectively. A detailed design and simulation, fabrication, and characterisation results are presented. The scheme demonstrates a scalable and efficient surface grating approach for polymer photonic integrated circuits.

1. Introduction

Polymer based photonic circuits have attracted considerable attention for a host of applications in sensing and communication. Application in sensing includes low-cost label-free fluid and biological sensing [1–3]. Polymer waveguides are used for chip-to-chip, intra-chip, as well as board-level optical interconnects for datacom applications [4–7]. Unlike conventional inorganic waveguide materials, polymers are relatively simple to process and incorporate functional optical components and circuits [8–10]. As opposed to high-index contrast waveguide platform such as SOI, sidewall scattering losses for polymer optical waveguides is considerably lower due to its low-index contrast [7,11,12]. However, the circuit footprint eventually becomes larger, which perhaps is a trade-off for loss and simplicity in the fabrication process. Polymer photonic circuits offer a versatile platform where one could tune the thermal, electrical, and optical property through doping. Tunable thermo-optic coefficients of polymers have allowed development of variable optical attenuators and tunable Bragg filters [13,14]. Similarly polymer materials can be doped with suitable chromophores to achieve high electro-optic coefficients of up to 5X higher than corresponding inorganic materials [15].

Compact and high-speed electro-optic modulators have already been demonstrated on planar hybrid polymer photonic platform [16,17]. Another major application is in the area of flexible photonics chips where the stretching feature of polymers is being explored for a host of applications such as flexible interconnects [18], substrate handles for high index materials [19,20] as well as strain sensing [21–25]. Lastly, a unique feature of polymers is the chemically induced optical birefringence, that can be incorporated to develop polarisation selective devices [26,27].

#412266 https://doi.org/10.1364/OE.412266
Journal © 2021 Received 12 Oct 2020; revised 1 Jan 2021; accepted 1 Feb 2021; published 15 Mar 2021

Optics EXPRESS

One of the challenges in polymer photonic circuits is achieving efficient coupling between an optical fibre and a single-mode polymer waveguides. Both in-plane, as well as out-of-plane coupling mechanisms, have been explored. The former technique, in-plane or edge coupling offers higher efficiency and broadband performance [28–30]. Also, due to a larger waveguide cross-section and low-index contrast, in-plane edge couplers to polymer waveguide intrinsically have higher misalignment tolerance. However, a significant drawback of this approach is a lack of scalable testing and high-volume manufacturing. Despite the advantages mentioned above, edge coupling requires consistent dicing and edge polished surface to avoid scattering loss. Due to higher modulus of elasticity, cleaving and polishing polymer waveguide is fundamentally limited. Thus out-of-plane coupling using surface diffraction grating is a scalable and suitable scheme for fibre-chip coupling. However, designing an efficient polymer grating is challenging due to the low-index contrast. Several means in the past have been suggested to address the low-index contrast such as by depositing high index contrast materials for gratings [31,32] or by using an air-suspended polymer membrane [33]. The reported efficiencies were modest with suboptimal performance. The efficiency could be increased by using thicker high-index material. This would enable higher diffractive efficiency and consequently, higher coupling performance. In addition, the coupling can further be boosted by implementing a bottom mirror to suppress substrate leakage and increase directionality that has been demonstrated in the case of SiO_2 clad SiN gratings [34–36].

In this work, we propose and demonstrate an efficient, scalable, and configurable grating-based coupling and polymer photonic circuit platform. The proposed approach couples light between a single-mode optical fibre and a *SU*8 waveguide using a combination of Silicon Nitride (*SiN*) grating and a spot size converter. A 3D schematic of the conceptual design is illustrated in Fig. 1. The design consists of two parts; a polymer encapsulated *SiN* grating for enabling coupling from a fibre to a *SiN* waveguide, and a hybrid polymer-*SiN* inverse taper to transfer the optical mode from the *SiN* waveguide to the single-mode polymer waveguide. The circuit is built on a silicon wafer with a silicon dioxide isolation layer. The proposed scheme uses an optimised *SiN* grating

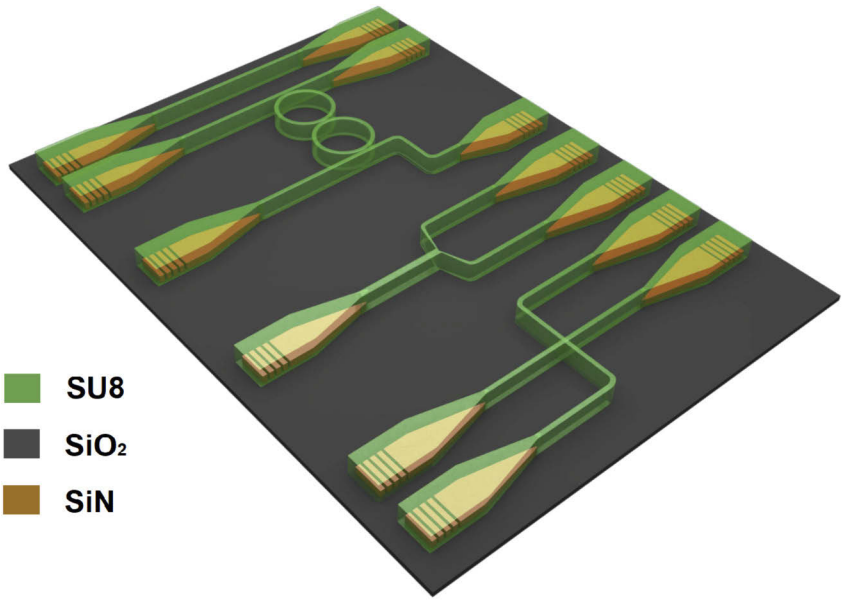

Fig. 1. 3D conceptual layout of a polymer photonic chip with the proposed configuration consisting of *SiN* gratings, spot size converter and *SU*8 guides and rings.

Optics EXPRESS

coupler as a generic coupling element that could be configured using a polymer waveguide to realise desired functionality. The proposal brings large volume CMOS compatible fabrication of *SiN* couplers with a configurable polymer waveguide platform. Using this approach, we demonstrate a maximum fibre-to-polymer waveguide coupling of 2.92 dB/coupler with a 3-dB bandwidth of 80 nm in the telecommunication L-band wavelength. To the best of our knowledge, the coupling efficiency achieved is the best reported for a grating fibre-chip coupler in a polymer waveguide platform.

2. Design and simulation

Figure 2(a) shows a schematic of various sections of the circuit that needs to be designed and optimised. In this section, we present the design and optimisation of various sections.

A commercially available photosensitive *SU*8 2002 is chosen as a polymer waveguide core material. The waveguide structure consists of an air-clad waveguide on a SiO_2 bottom clad on the silicon handle substrate. *SU*8 is a versatile photosensitive polymer and has broad transparency (400-2000 nm). Depending on the resist viscosity and spin coating parameters, the core film thickness can be tuned between 1 to 3 μm. Single-mode polymer waveguide is designed and simulated using MODE [37]. Simulations are performed at 1550 nm wavelength, and a refractive index of 1.575 and 1.45 is used for *SU*8 and SiO_2, respectively. Figure 2(b) shows the waveguide dispersion of a 2 μm thick *SU*8 polymer layer. Based on the waveguide dispersion, a core dimension of 2×2 μm is used as a single-mode waveguide.

2.1. Inverse taper design

The coupling between an optical fibre and the polymer waveguide is done using a *SiN* grating and a taper section. The grating coupler and the taper section is defined in a 400 nm thick *SiN* layer to operate in a single-mode regime. To spatially mode match with a single-mode fibre the grating is defined in a 12 μm wide waveguide. Coupling between the broad waveguide and the polymer waveguide is achieved using inverse taper as depicted in Fig. 2(a).

The inverse taper design was optimized using the eigenmode mode expansion (EME) solvers [37,38]. The 2D layout of the proposed design stack and its various components is illustrated in Fig. 2(c). The first stage consists of a SiN patch grating that is 12 μm wide and of length L_1. In the second stage, the fundamental *TE* mode from the 12 μm wide *SiN* waveguide is channelled through an adiabatic two-stage section. In the first section, the 12 μm wide waveguide is tapered to 1 μm wide waveguide through an adiabatic taper, followed by a second stage, where an inverse taper is used to couple light to the overlaid polymer waveguide. The inverse tapering allows the light to leak into the single-mode *SU*8 waveguide present on top. The total power transmitted to the *TE* mode in the *SU*8 guide is estimated through the scattering matrix of the composite structure. The taper section is optimized in two stages. In the first optimization step, a maximum transmitted between the fundamental *TE* mode in patch waveguide to the corresponding 1 μm wide *SiN* waveguide through an adiabatic taper L_2 is achieved. In the second step, maximum transmission between the 1 μm wide *SiN* waveguide and the 2 μm wide *SU*8 through the inverse taper L_3 is optimized.

Figure 3(a) shows the transmission of the first stage L_2 taper as a function of length. An L_2 of 300 μm yielding a conversion efficiency of > -0.05 dB, is fixed thereafter as the optimum intermediate taper. Figure 3(b) shows the power transmission as a function of *SiN* inverse taper tip width and length L_3. Optimisation with both proprietary solvers shows an excellent agreement in optimal length and taper width. We achieve a maximum transmission loss of -0.04 dB or a transmission efficiency of 99 % for a tip width of 75 nm and L_3 of 100 μm. Even with a tip width of 100 nm, a transmission loss of -0.06 dB is achieved. Both these tip dimensions are feasible with ArF-immersion lithography. As the tip width increases to 150 nm and 200 nm, we observe an increase in the transmission loss to -0.1 and -0.2 dB/facet respectively, due to mode mismatch

Optics EXPRESS

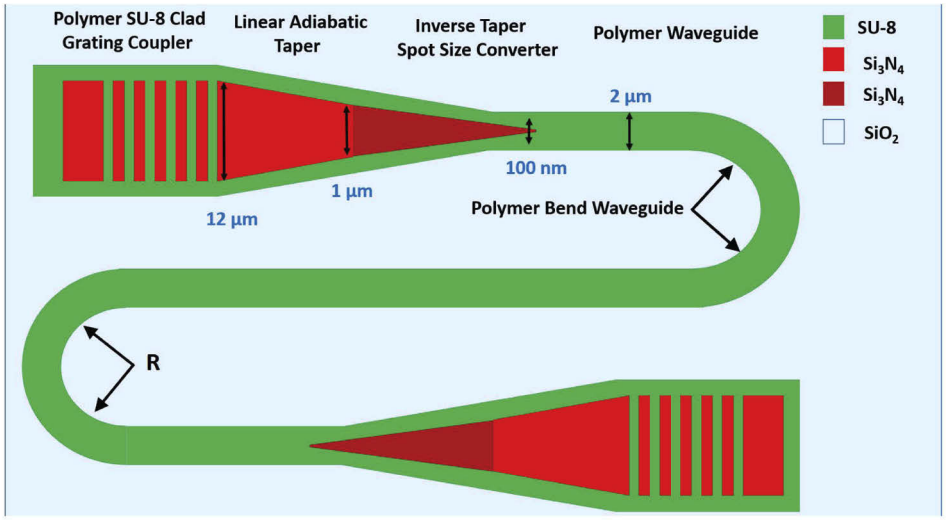

(a)

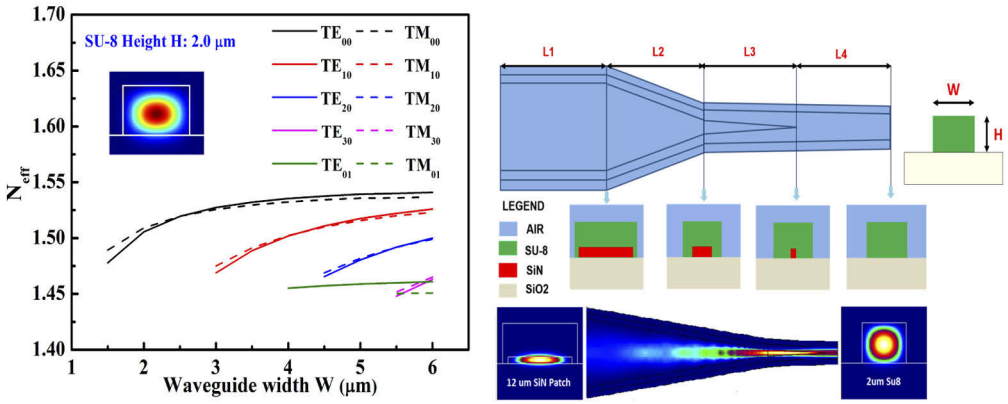

(b) (c)

Fig. 2. (a) illustrates 2D cross section of the proposed hybrid *SiN*/*SU*8 grating coupler inverse taper. (b) shows waveguide dispersion of effective mode index N_{eff} at different widths W for *SU*8 film thickness of 2 μm. The inset shows the electric field intensity profile for the fundamental TE_{00} mode for a core dimension of 2×2 μm. (c) shows simulated layout and cross-section along the taper length. Also depicted is the *SU*8 waveguide width W and height HThe cross-sectional field plot at the either end shows TE_{00} mode evolution from *SiN* patch core to the *SU*8 waveguide core.

between the taper and the polymer waveguide. To achieve higher transmission efficiency tip widths <200 nm is desirable, which can be fabricated with standard DUV lithography [39–41]. The oscillatory fluctuation of the mode conversion loss with L_3 taper length is due to the cumulative effect of partial reflections at infinitesimal slices along the taper. These oscillations are observed to be more pronounced for higher taper widths [42]. For tip widths < 200 nm, we observe that, L_3 as short as 50 μm is sufficient to achieve transmission > -0.5 dB. Since the present design is unconstrained by footprint, we choose an L_3 of 100 μm as optimum inverse taper length.

Optics EXPRESS

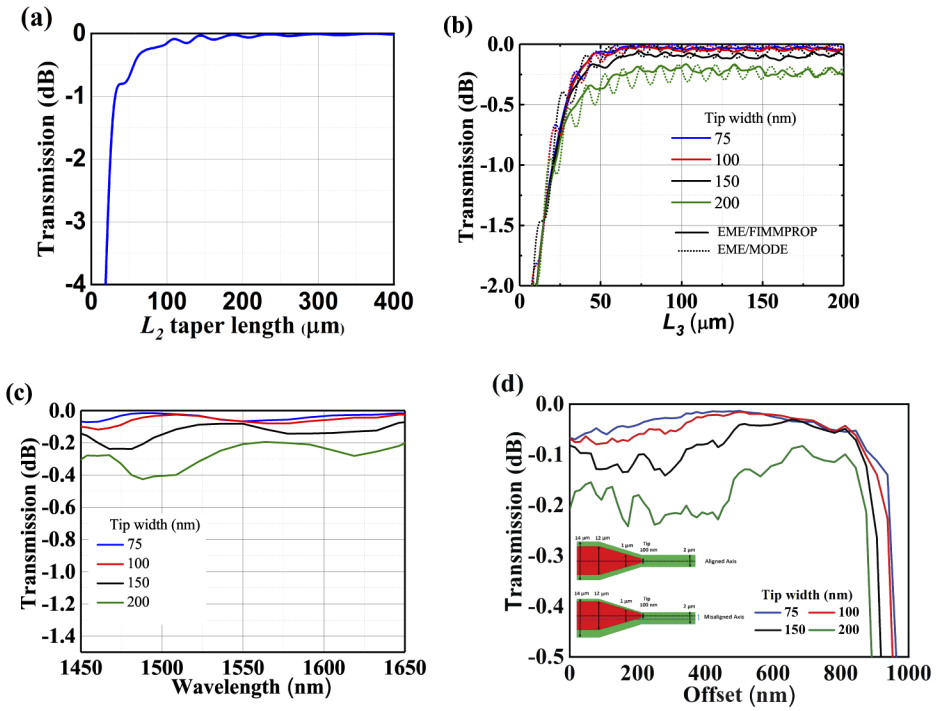

Fig. 3. (a) plots the adiabatic conversion efficiency of taper section L_2, (b) shows a comparison of inverse taper conversion efficiency as a function of parameter L_3 as simulated for both FIMMPROP and MODE solver, (c) shows the bandwidth performance of tip widths at L_3 length 100 μm, and (d) showcases the offset dependence of taper conversion at different tip widths.

Figure 3(c) shows the spectral characteristics of 100 μm long L_3 with various tip widths. The overall transmission is observed to be flat over SCL band (1450-1650 nm) with a transmission ripple of < 0.1 dB. The design offers a broadband operation with a transmission bandwidth of over 200 nm, which is essential for a wavelength scalable circuit design. The total length of the taper ($L_1 + L_2 + L_3$), for an efficiency transmission is about 420 μm. The length of this taper could be reduced by using a compact non-adiabatic taper, that could reduce the taper length by 50 % [43].

The polymer waveguide would be defined in a separate lithography step that may result in misalignment between the *SiN* inverse taper and the polymer waveguide. Figure 3(d) shows the effect of misalignment or offset between the taper and the polymer waveguide. We find a robust alignment tolerant transmission for tip widths of <200 nm. However, for misalignment >800 nm there is a steep increase in the transmission loss. An alignment overlay accuracy better than 800 nm is easily achievable even in a contact lithography system. The robustness in design and alignment tolerance between the *SiN* and the polymer layer clearly indicates the feasibility of a configurable platform where the *SiN* based generic coupler layout could manufacture using large volume CMOS patterning process. In contrast, the polymer circuit could be done using a simple contact lithography system as well.

2.2. Grating design

The *SiN* grating is optimised using 2D simulations using a finite-difference-time-domain (FDTD) solver from [37]. A cross-section schematic of the *SU*8 cladded *SiN* grating coupler is depicted

Optics EXPRESS

in Fig. 4(a). The grating in the *SiN* is designed to phase match with the fundamental propagating TE-mode of the *SiN* waveguide. For efficient coupling, we use a bottom reflector to improve directionality. According to the first-order Bragg phase-matching condition, the grating period Λ

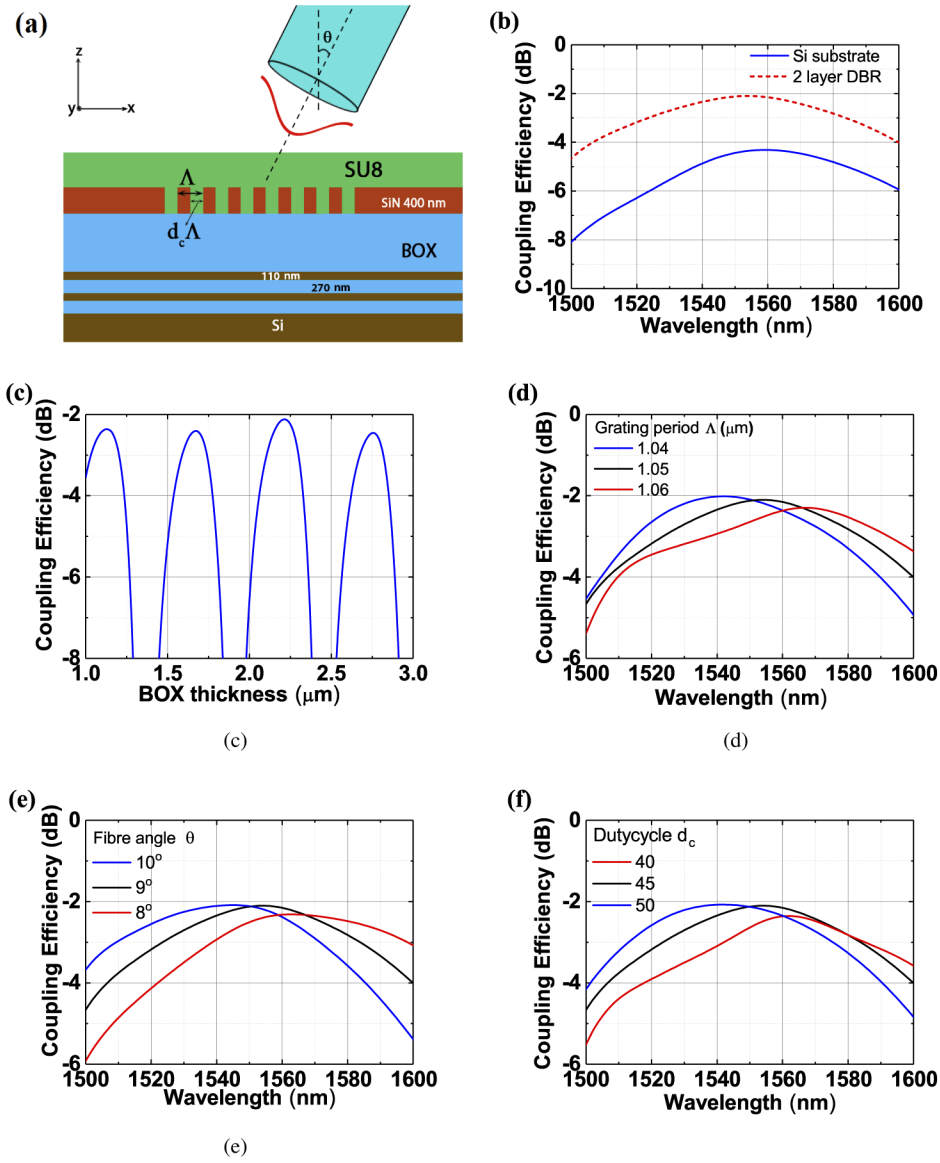

Fig. 4. (a) 2D cross section of the hybrid *SiN*-*SU*8 grating coupler with a DBR stack used in FDTD simulations, (b) shows simulated coupling efficiency of *SU*8 coated *SiN* grating couplers, with and without a DBR stack, used in FDTD simulations at 1.05 μm period, (c) shows simulated coupling efficiency as a function of BOX thickness at 1550 nm for 1.05 μm grating period with a DBR stack, (d) depicts coupling as a function of different periods at 45 % d_c, 9° incident angle, (e) and (f) shows the coupling performance at 1.05 μm period for different angles and duty-cycles respectively.

Optics EXPRESS

can be expressed as:

$$\Lambda = \frac{\lambda}{N_{eff}^{g} - n_c sin(\theta)} \tag{1}$$

Where N_{eff}^{g} is the effective grating index, n_c is the cladding index, and θ is the angle of incidence. N_{eff}^{g} is estimated from the relation N_{eff}^{g}=$d_c N_{etch} + (1 - d_c)N_{eff}^{TE}$. Here N_{eff}^{TE} and N_{etch} are the effective *TE* mode indices of the slab and etched portions, respectively, and d_c is the duty-cycle. The refractive indices of *SU*8, SiO_2, *SiN*, amorphous $a - Si$ and crystalline *c-Si* were taken as 1.575, 1.44, 2.015, 3.53, and 3.46, respectively. A Gaussian source of 10.4 μm mode field diameter (MFD) is used as an illuminating source above the *SU*8 cladding). All the grating parameters such as Λ, θ, d_c, and buried oxide thickness (BOX) are optimised to achieve maximum coupling to the *SiN* waveguide. For a simple *SiN* fabrication process, a single full 400 nm etch for both grating and waveguide is considered. Grating coupling efficiency is initially optimised with a just an oxide bottom clad layer on a *Si* substrate. Figure 4(b) compares the impact on coupling efficiency of the polymer clad *SiN* grating, with and without a the bottom reflector. For the case of no reflector, peak coupling efficiency at C-band is observed to be -4.3 dB with a 1-dB bandwidth of 56 nm at a period of 1.05 μm and 9° inclination. The coupling efficiency can be further improved by suppressing substrate leakage by incorporating a bottom reflector beneath the BOX layer, such as a distributed Bragg reflector (DBR). The DBR stack consists of 2 cascaded layers of $a - Si/SiO_2$, with a quarter-wave thickness of 110/270 nm. At an optimal BOX thickness, constructive interference occurs between the substrate reflected and the upper diffracted light from the DBR, which results in a higher directionality. With a 2-pair of reflector stack, the coupling efficiency is improved to -2.14 dB with a 1 and 3 dB bandwidths of 64 nm and 114 nm respectively. Since improvement in the coupling efficiency is achieved by phase-matching, the reflected and diffracted light from the grating, the BOX thickness is critical. Figure 4(c) depicts the effect of BOX thickness on the coupling efficiency. The optimal BOX thickness for the gratings is found to be 2.22 μm. For a BOX thickness variation of ±80 nm, we observe the coupling penalty to be only -0.8 dB. The effect of grating period, fibre inclination angles and duty-cycles is plotted in Figs. 4(d)-(f) respectively. Based on the optimisation, optimal grating parameters is chosen for device fabrication.

3. Device fabrication and characterization

Device fabrication was carried on a standard *Si* wafer. A two-layer Bragg reflector of 270 nm SiO_2 and 110 nm thick $a - Si$ is deposited using Plasma Enhanced Chemical Vapour Deposition (PECVD). This is followed by depositing 2.22 μm thick SiO_2 and then a 400 nm thick *SiN* layer also using the PECVD process. Following the layer deposition grating and waveguide patterning is performed using e-beam lithography. Gratings of different periods and duty-cycles along with inverse tapers are patterned using a negative tone resist (MaN-2403). The inverse taper tip width is fixed at 100 nm for all devices. The *SiN* layer was then fully etched using inductively coupled plasma reactive ion etching (ICP-RIE) with SF6 chemistry. Subsequently, a 2 μm thick *SU*8 2002 photosensitive polymer is spin-coated on this etched pattern. Figure 5 depicts the detailed process flow for the fabricated devices.

The gratings are connected by pattering the *SU*8 layer. The photosensitive polymer could be either patterned using direct-laser writer or optical projection/contact lithography. In this work, we use a direct-write scheme to demonstrate a configurable polymer photonic circuit. The direct-write process is optimised to achieve low-loss smooth *SU*8 waveguides [44,45]. The test structures were fabricated with straight polymer waveguides. Following the writing process, the waveguides are developed and baked at 65° C and 95° C for one and four minutes, respectively. Subsequently, the sample was thermally cured at 175° C for 15 minutes to remove the solvents. Figure 6(a) depicts test structures fabricated using the direct-writing process. Figures 6(b) and

Optics EXPRESS

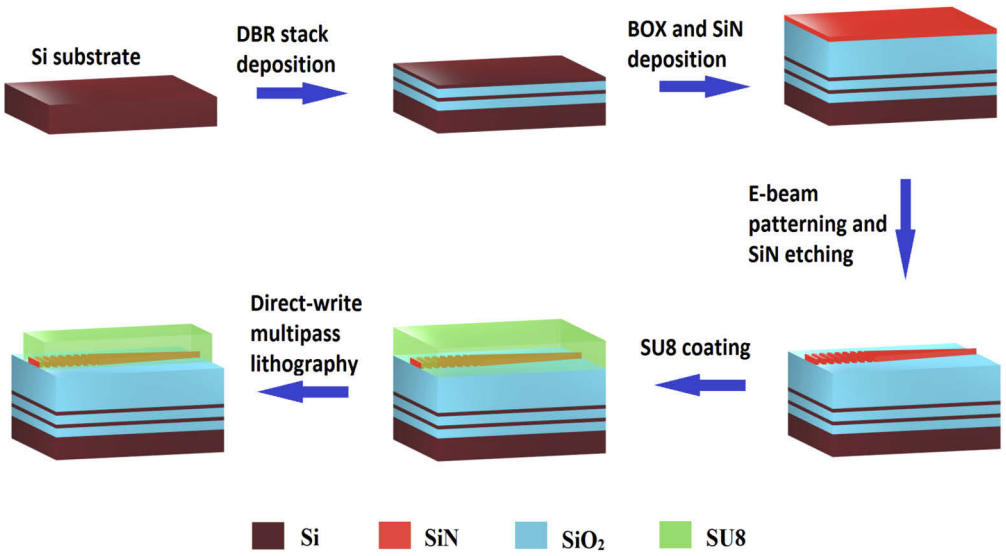

Fig. 5. Process flow schematic of the fabricated devices.

(c) show the cross-sections of a fabricated grating with bottom reflector and the *SU*8 patterned waveguide respectively.

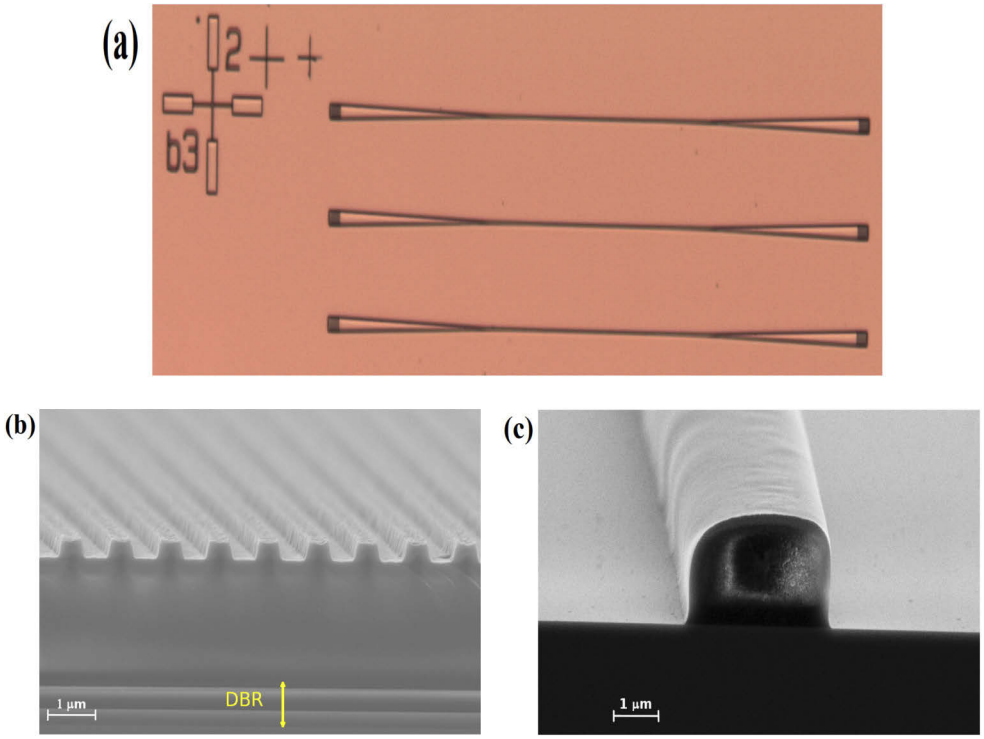

Fig. 6. (a) shows the top microscope image of some of the patterned *SU*8 structures with straight waveguides. (b) and (c) show the side view SEM cross-section of (b), the *SiN* grating region with the DBR stack prior to *SU*8 coating and (c), the *SU*8 waveguide.

Optics EXPRESS

The fabricated devices were characterized using a tunable laser (Keysight 81690A) and a photodetector (Keysight 81636B). The characterization summary is shown in Fig. 7. Here, Figs. 7(a)-(b) and Figs. 7(c)-(d) show the effect of the grating period and fibre inclination angle on the fibre-to-*SU*8 coupling efficiency in the C-band and L-band, respectively. We measure a maximum coupling efficiency of -3.55 dB/coupler (at 1560 nm) with 74 nm of 3-dB bandwidth in the C-band. While in the L-band, we measure a maximum efficiency of -2.92 dB/coupler (at 1603 nm) with a 3-dB bandwidth of close to 80 nm. The maximum efficiency is achieved with a grating period, duty cycle and fibre angle combination of 1.05 μm, 50 %, 8° and 1.04 μm, 45 % and 5° for C- band and L-band couplers, respectively. Table 1 summarizes the type and performance metric of various surface grating schemes demonstrated for polymer waveguide coupling.

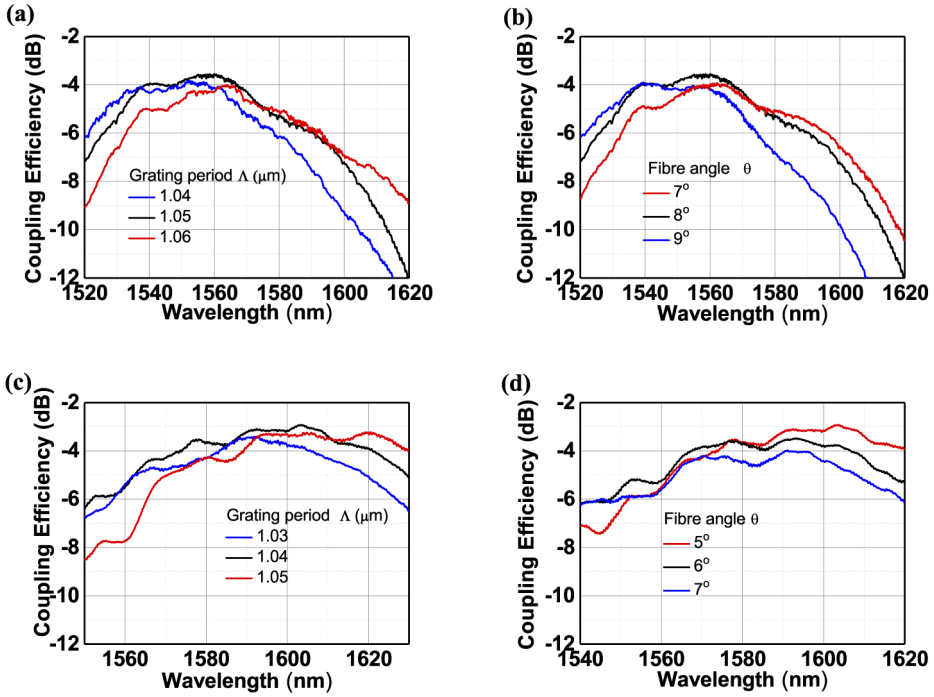

Fig. 7. (a)-(b) shows measured coupling to straight *SU*8 waveguides at C-band for (a) different periods at 8° inclination and (b) different angles for 1.05 μm period and 50 % d_c. (c)-(d) depict measured spectrum at L-band for (c) different periods at 5° inclination and 45 % d_c and (d) for different angles at 1.04 μm period.

It may be pointed out that although we have used electron beam and direct-write lithography, the design allows flexibility in determining minimum feature dimensions that is compatible with scalable, high-volume optical lithography typically employed in foundries. The proposed device can serve as a suitable template for developing on-chip PCB interconnects [6] as well as a substrate handle for flexible polymer circuits [19].

Optics EXPRESS

Table 1. Performance comparison of surface grating couplers demonstrated on various polymer waveguide platforms.[a]

Reference	Max. CE (dB)	$\delta\lambda_{3dB}$ (nm)	λ_{max} (nm)	N_{HI}/N_{LI}	Taper Length	t_{HI} (nm)	Bottom Reflector
Ref. [31]	-9.5	-	1550	2/1.65	-	140	N
Ref. [32]	-8.6	32	1550	1.84/1.52	5 mm	200	N
Ref. [33]	-8.0	-	1557	1.57/1	-	600	N
This work	**-3.55**	**74**	**1560**	**2.015/1.57**	**840 μm**	**400**	**Y**
This work	**-2.92**	**80**	**1603**	**2.015/1.57**	**840 μm**	**400**	**Y**

[a]HI = high optical index, LI = low optical index material.

4. Conclusion

We demonstrate a low-loss coupling scheme between a single-mode optical fibre and a single-mode polymer waveguide using *SiN* grating coupler. A detailed design, simulation, fabrication, and characterisation of the proposed scheme is presented. The grating couplers in *SiN* offers a flexible platform for building polymer circuits. Using the proposed approach, we demonstrate a maximum coupling efficiency of -3.55 and -2.92 dB to a single-mode *SU*8 waveguide in C and L band region, respectively. The proposed configurable platform offers flexibility is pattering the polymer waveguide without any constrains on the light-chip coupler. A generic predefined *SiN* coupler could be mass-fabricated and used as a platform for polymer circuit fabrication. The results hold promise for realising a scalable and efficient surface grating approach for polymer photonic integrated circuits.

Funding. Ministry of Human Resource Development; Ministry of Electronics and Information technology; Mission on Nano Science and Technology.

Acknowledgements. We thank Department of Science and Technology, Science and Engineering Board for funding this research. We also acknowledge funding support from MHRD through NIEIN project, from MeitY and DST through NNetRA. We thank Mr Subhash K M for his technical support for the device fabrication.

Disclosures. The authors declare no conflicts of interest.

References

1. J. Ren, L. Wang, X. Han, J. Cheng, H. Lv, J. Wang, X. Jian, M. Zhao, and L. Jia, "Organic Silicone Sol-Gel Polymer as a Noncovalent Carrier of Receptor Proteins for Label-Free Optical Biosensor Application," ACS Appl. Mater. Interfaces **5**(2), 386–394 (2013).
2. J. Kim, K. Kim, J. Yi, and M. Oh, "Polymer Waveguide Label-Free Biosensors With Enhanced Sensitivity by Incorporating Low-Refractive-Index Polymers," IEEE J. Sel. Top. Quantum Electron. **16**(4), 973–980 (2010).
3. M. Ramuz, D. Leuenberger, and L. Bürgi, "Optical biosensors based on integrated polymer light source and polymer photodiode," J. Polym. Sci. Part B Polym. Phys. **49**(1), 80–87 (2011).
4. X. Zhang, A. Hosseini, X. Lin, H. Subbaraman, and R. T. Chen, "Polymer-Based Hybrid-Integrated Photonic Devices for Silicon On-Chip Modulation and Board-Level Optical Interconnects," IEEE J. Sel. Top. Quantum Electron. **19**(6), 196–210 (2013).
5. R. Pitwon, M. Immonen, K. Wang, H. Itoh, T. Shioda, J. Wu, L. X. Zhu, H. J. Yan, and A. Worrall, "International standards for optical circuit board fabrication, assembly and measurement," Opt. Commun. **362**, 22–32 (2016).
6. R. Kallega, S. Nambiar, A. Kumar, P. Ranganath, and S. K. Selvaraja, "Silicon photonic IC embedded optical-PCB for high-speed interconnect application," in *Opt. Interconnects XVIII*, vol. 10538 H. Schröder and R. T. Chen, eds., International Society for Optics and Photonics (SPIE, 2018), pp. 79–84.
7. R. Dangel, J. Hofrichter, F. Horst, D. Jubin, A. L. Porta, N. Meier, I. M. Soganci, J. Weiss, and B. J. Offrein, "Polymer waveguides for electro-optical integration in data centers and high-performance computers," Opt. Express **23**(4), 4736–4750 (2015).
8. H. Ma, A.-Y. Jen, and L. R. Dalton, "Polymer-Based Optical Waveguides: Materials, Processing, and Devices," Adv. Mater. **14**(19), 1339–1365 (2002).
9. X.-Y. Han, Z.-L. Wu, S.-C. Yang, F.-F. Shen, Y.-X. Liang, L.-H. Wang, J.-Y. Wang, J. Ren, L.-Y. Jia, H. Zhang, S.-H. Bo, G. Morthier, and M.-S. Zhao, "Recent Progress of Imprinted Polymer Photonic Waveguide Devices and Applications," Polymers **10**(6), 603 (2018).

Optics EXPRESS

10. T. Ishigure and Y. Nitta, "Polymer optical waveguide with multiple graded-index cores for on-board interconnects fabricated using soft-lithography," Opt. Express **18**(13), 14191–14201 (2010).
11. M. Nordstrom, D. A. Zauner, A. Boisen, and J. Hubner, "Single-mode waveguides with su-8 polymer core and cladding for moems applications," J. Lightwave Technol. **25**(5), 1284–1289 (2007).
12. A. Marinins, N. Knudde, and S. Popov, "Air-suspended su-8 strip waveguides with high refractive index contrast," IEEE Photonics Technol. Lett. **28**(17), 1862–1865 (2016).
13. Z. Zhang and N. Keil, "Thermo-optic devices on polymer platform," Opt. Commun. **362**, 101–114 (2016).
14. A. Liu, Z. Zhang, D. de Felipe, N. Keil, and N. Grote, "Power-Efficient Thermo-Optic Tunable Filters Based on Polymeric Waveguide Bragg Gratings," IEEE Photonics Technol. Lett. **26**(3), 313–315 (2014).
15. Y. Enami, C. T. Derose, D. Mathine, C. Loychik, C. Greenlee, R. A. Norwood, T. D. Kim, J. Luo, Y. Tian, A. K.-Y. Jen, and N. Peyghambarian, "Hybrid polymer/sol-gel waveguide modulators with exceptionally large electro-optic coefficients," Nat. Photonics **1**(3), 180–185 (2007).
16. Z. Pan, X. Xu, C.-J. Chung, H. Dalir, H. Yan, K. Chen, Y. Wang, B. Jia, and R. T. Chen, "High-Speed Modulator Based on Electro-Optic Polymer Infiltrated Subwavelength Grating Waveguide Ring Resonator," Laser Photonics Rev. **12**(6), 1700300 (2018).
17. M. Lee, H. E. Katz, C. Erben, D. M. Gill, P. Gopalan, J. D. Heber, and D. J. McGee, "Broadband Modulation of Light by Using an Electro-Optic Polymer," Science **298**(5597), 1401–1403 (2002).
18. L. Li, Y. Zou, H. Lin, J. Hu, X. Sun, N. Feng, S. Danto, K. Richardson, T. Gu, and M. Haney, "A Fully-Integrated Flexible Photonic Platform for Chip-to-Chip Optical Interconnects," J. Lightwave Technol. **31**(24), 4080–4086 (2013).
19. R. Kallega, S. Nambiar, S. Kalathimekkad, V. Mere, and S. K. Selvaraja, "Flexible silicon nitride photonic integrated circuit embedded in polymer handle," in *Integr. Opt. Devices, Mater. Technol. XXIII*, vol. 10921 S. M. García-Blanco and P. Cheben, eds., International Society for Optics and Photonics (SPIE, 2019), pp. 52–56.
20. H. Zuo, S. Yu, T. Gu, and J. Hu, "Low loss, flexible single-mode polymer photonics," Opt. Express **27**(8), 11152–11159 (2019).
21. L. Li, H. Lin, S. Qiao, Y. Z. Huang, J. Y. Li, J. Michon, T. Gu, C. Alosno-Ramos, L. Vivien, A. Yadav, K. Richardson, N. Lu, and J. Hu, "Monolithically integrated stretchable photonics," Light: Sci. Appl. **7**(2), 17138 (2018).
22. J. Missinne, N. Teigell Benéitez, A. Lamberti, G. Chiesura, G. Luyckx, M.-A. Mattelin, W. Van Paepegem, and G. Van Steenberge, "Thin and Flexible Polymer Photonic Sensor Foils for Monitoring Composite Structures," Adv. Eng. Mater. **20**(6), 1701127 (2018).
23. L. Fan, L. T. Varghese, Y. Xuan, J. Wang, B. Niu, and M. Qi, "Direct fabrication of silicon photonic devices on a flexible platform and its application for strain sensing," Opt. Express **20**(18), 20564–20575 (2012).
24. W. Peng and H. Wu, "Flexible and Stretchable Photonic Sensors Based on Modulation of Light Transmission," Adv. Opt. Mater. **7**(12), 1900329 (2019).
25. S. Yun, S. Park, B. Park, Y. Kim, S. K. Park, S. Nam, and K.-U. Kyung, "Polymer-Waveguide-Based Flexible Tactile Sensor Array for Dynamic Response," Adv. Mater. **26**(26), 4474–4480 (2014).
26. J. Kim, K. Kim, M. Oh, J. Seo, Y. Noh, and H. Lee, "Polarization-Splitting Waveguide Devices Incorporating Perfluorinated Birefringent Polymers," J. Lightwave Technol. **29**(12), 1842–1846 (2011).
27. A. Tagaya, H. Ohkita, T. Harada, K. Ishibashi, and Y. Koike, "Zero-Birefringence Optical Polymers," Macromolecules **39**(8), 3019–3023 (2006).
28. Ashley Sanghadasa, Cocke Webster, and Guenthner Lindsay, "A simplified technique for efficient fiber-polymer-waveguide power coupling using a customized cladding with tunable index of refraction," J. Lightwave Technol. **24**(10), 3816–3823 (2006).
29. A. Rashidi, R. Gharavi, and A. Gharavi, "Fiber to polymer-waveguide coupling with low insertion loss," J. Opt. **17**(4), 045801 (2015).
30. Z. Pan, H. Subbaraman, Y. Zou, X. Xu, X. Zhang, C. Zhang, Q. Li, L. J. Guo, and R. T. Chen, "Quasi-vertical tapers for polymer-waveguide-based interboard optical interconnects," Photonics Res. **3**(6), 317–323 (2015).
31. R. Bruck and R. Hainberger, "Efficient coupling of narrow beams into polyimide waveguides by means of grating couplers with high-index coating," Appl. Opt. **49**(10), 1972–1978 (2010).
32. L. Wang, Y. Li, M. Garcia Porcel, D. Vermeulen, X. Han, J. Wang, X. Jian, R. Baets, M. Zhao, and G. Morthier, "A polymer-based surface grating coupler with an embedded Si3N4 layer," J. Appl. Phys. **111**(11), 114507 (2012).
33. C. Prokop, S. Schoenhardt, B. Laegel, S. Wolff, A. Mitchell, and C. Karnutsch, "Air-Suspended SU-8 Polymer Waveguide Grating Couplers," J. Lightwave Technol. **34**(17), 3966–3971 (2016).
34. C. R. Doerr, L. Chen, Y. K. Chen, and L. L. Buhl, "Wide Bandwidth Silicon Nitride Grating Coupler," IEEE Photonics Technol. Lett. **22**(19), 1461–1463 (2010).
35. H. Zhang, C. Li, X. Tu, J. Song, H. Zhou, X. Luo, Y. Huang, M. Yu, and G. Q. Lo, "Efficient silicon nitride grating coupler with distributed Bragg reflectors," Opt. Express **22**(18), 21800–21805 (2014).
36. S. Nambiar, A. Kumar, R. Kallega, P. Ranganath, and S. K. Selvaraja, "High-Efficiency Grating Coupler in 400 nm and 500 nm PECVD Silicon Nitride With Bottom Reflector," IEEE Photonics J. **11**(5), 1–13 (2019).
37. "Ansys/Lumerical," Ansys/Lumerical, https://www.lumerical.com/.
38. "Photon design," Photon Design, https://www.photond.com/.

Optics EXPRESS

39. S. K. Selvaraja, G. Winroth, S. Locorotondo, G. Murdoch, A. Milenin, C. Delvaux, P. Ong, S. Pathak, W. Xie, G. Sterckx, G. Lepage, D. V. Thourhout, W. Bogaerts, J. V. Campenhout, and P. Absil, "193nm immersion lithography for high-performance silicon photonic circuits," Proc. SPIE **9052**, 90520F (2014).
40. J. H. Song, T. D. Kongnyuy, B. Troia, S. S. Saseendran, P. Soussan, R. Jansen, and X. Rottenberg, "Grating devices on a silicon nitride technology platform for visible light applications," OSA Continuum **2**(4), 1155–1165 (2019).
41. T. Horikawa, D. Shimura, H. Okayama, S. Jeong, H. Takahashi, J. Ushida, Y. Sobu, A. Shiina, M. Tokushima, K. Kinoshita, and T. Mogami, "A 300-mm silicon photonics platform for large-scale device integration," IEEE J. Sel. Top. Quantum Electron. **24**(4), 1–15 (2018).
42. M. Wood, P. Sun, and R. M. Reano, "Compact cantilever couplers for low-loss fiber coupling to silicon photonic integrated circuits," Opt. Express **20**(1), 164–172 (2012).
43. P. Sethi, R. Kallega, A. Haldar, and S. K. Selvaraja, "Compact broadband low-loss taper for coupling to a silicon nitride photonic wire," Opt. Lett. **43**(14), 3433–3436 (2018).
44. J. C. Ramirez, J. N. Schianti, M. G. Almeida, A. Pavani, R. R. Panepucci, H. E. Hernandez-Figueroa, and L. H. Gabrielli, "Low-loss modified SU-8 waveguides by direct laser writing at 405 nm," Opt. Mater. Express **7**(7), 2651–2659 (2017).
45. M. Schumann, T. Bückmann, N. Gruhler, M. Wegener, and W. Pernice, "Hybrid 2D-3D optical devices for integrated optics by direct laser writing," Light: Sci. Appl. **3**(6), e175 (2014).